ARMY RESEARCH LABORATORY

Further Developments in Improved Sensitivity, Low-cost Uncooled IR Detector Focal Plane Arrays

by Wendy L. Sarney, John W. Little, Kimberley A. Olver, Frank E. Livingston, Krisztian Niesz, and Daniel E. Morse

ARL-TR-5389 **November 2010**

NOTICES

Disclaimers

The findings in this report are not to be construed as an official Department of the Army position unless so designated by other authorized documents.

Citation of manufacturer's or trade names does not constitute an official endorsement or approval of the use thereof.

Destroy this report when it is no longer needed. Do not return it to the originator.

Army Research Laboratory
Adelphi, MD 20783-1197

ARL-TR-5389 **November 2010**

Further Developments in Improved Sensitivity, Low-cost Uncooled IR Detector Focal Plane Arrays

Wendy L. Sarney, John W. Little, and Kimberley A. Olver
Sensors and Electron Devices Directorate, ARL

Frank E. Livingston
The Aerospace Corporation

Krisztian Niesz and Daniel E. Morse
Institute for Collaborative Biotechnologies,
University of California, Santa Barbara

REPORT DOCUMENTATION PAGE

Form Approved
OMB No. 0704-0188

1. REPORT DATE *(DD-MM-YYYY)*	2. REPORT TYPE	3. DATES COVERED (From - To)
November 2010	Final	May 1, 2009–July 30, 2009

4. TITLE AND SUBTITLE
Further Developments in Improved Sensitivity, Low-cost Uncooled IR Detector Focal Plane Arrays

5a. CONTRACT NUMBER

5b. GRANT NUMBER

5c. PROGRAM ELEMENT NUMBER

6. AUTHOR(S)
Wendy L. Sarney, John W. Little, Kimberley A. Olver, Frank E. Livingston, Krisztian Niesz, and Daniel E. Morse

5d. PROJECT NUMBER

5e. TASK NUMBER

5f. WORK UNIT NUMBER

7. PERFORMING ORGANIZATION NAME(S) AND ADDRESS(ES)
U.S. Army Research Laboratory
ATTN: RDRL-SEE-I
2800 Powder Mill Road
Adelphi, MD 20783-1197

8. PERFORMING ORGANIZATION REPORT NUMBER
ARL-TR-5389

9. SPONSORING/MONITORING AGENCY NAME(S) AND ADDRESS(ES)
Army Research Office
PO Box 12211
Research Triangle Park, NC 27709

10. SPONSOR/MONITOR'S ACRONYM(S)

11. SPONSOR/MONITOR'S REPORT NUMBER(S)

12. DISTRIBUTION/AVAILABILITY STATEMENT
Approved for public release; distribution unlimited.

13. SUPPLEMENTARY NOTES

14. ABSTRACT

The program goals for year 2-quarter 1 (Y2Q1) Institute for Collaborative Biotechnologies project 'Lower Cost Uncooled IR Detector Focal Plane Arrays' included (1) the continued expansion of our barium titanium oxide ($BaTiO_3$) nanomaterial synthesis capabilities and deposition methods, (2) laser-induced pyroelectric phase conversion studies and spectroscopic end-point control scheme, and (3) comprehensive material characterization studies, along with electrical property characterization of $BaTiO_3$ thin films. This report covers progress that took place in the three month period from May 1, 2009–July 30, 2009.

15. SUBJECT TERMS
Nanoparticles, uncooled infrared, biologically inspired

16. SECURITY CLASSIFICATION OF:			17. LIMITATION OF ABSTRACT	18. NUMBER OF PAGES	19a. NAME OF RESPONSIBLE PERSON
a. REPORT	b. ABSTRACT	c. THIS PAGE	UU	26	Wendy L. Sarney
Unclassified	Unclassified	Unclassified			19b. TELEPHONE NUMBER (*Include area code*) (301) 394-5761

Standard Form 298 (Rev. 8/98)
Prescribed by ANSI Std. Z39.18

Contents

List of Figures

List of Tables

Acknowledgments

We acknowledge support by the Institute for Collaborative Biotechnologies (ICB) through grant DAAD19-03-D-0004 from the U.S. Army Research Office, and The Aerospace Corporation Independent Research and Development (IR&D) Program and the Product and Development (PDP) Program.

INTENTIONALLY LEFT BLANK.

1. Introduction

The program goals for year 2-quarter 1 (Y2Q1) corresponded to the continued expansion of our barium titanium oxide ($BaTiO_3$) nanomaterial synthesis capabilities and deposition methods, laser-induced pyroelectric phase conversion studies and spectroscopic end-point control scheme, and comprehensive material characterization studies, along with electrical property characterization of $BaTiO_3$ thin films. This work took place in the three month period from May 1, 2009–July 30, 2009. The project schedule for year 2 is summarized in figure 1.

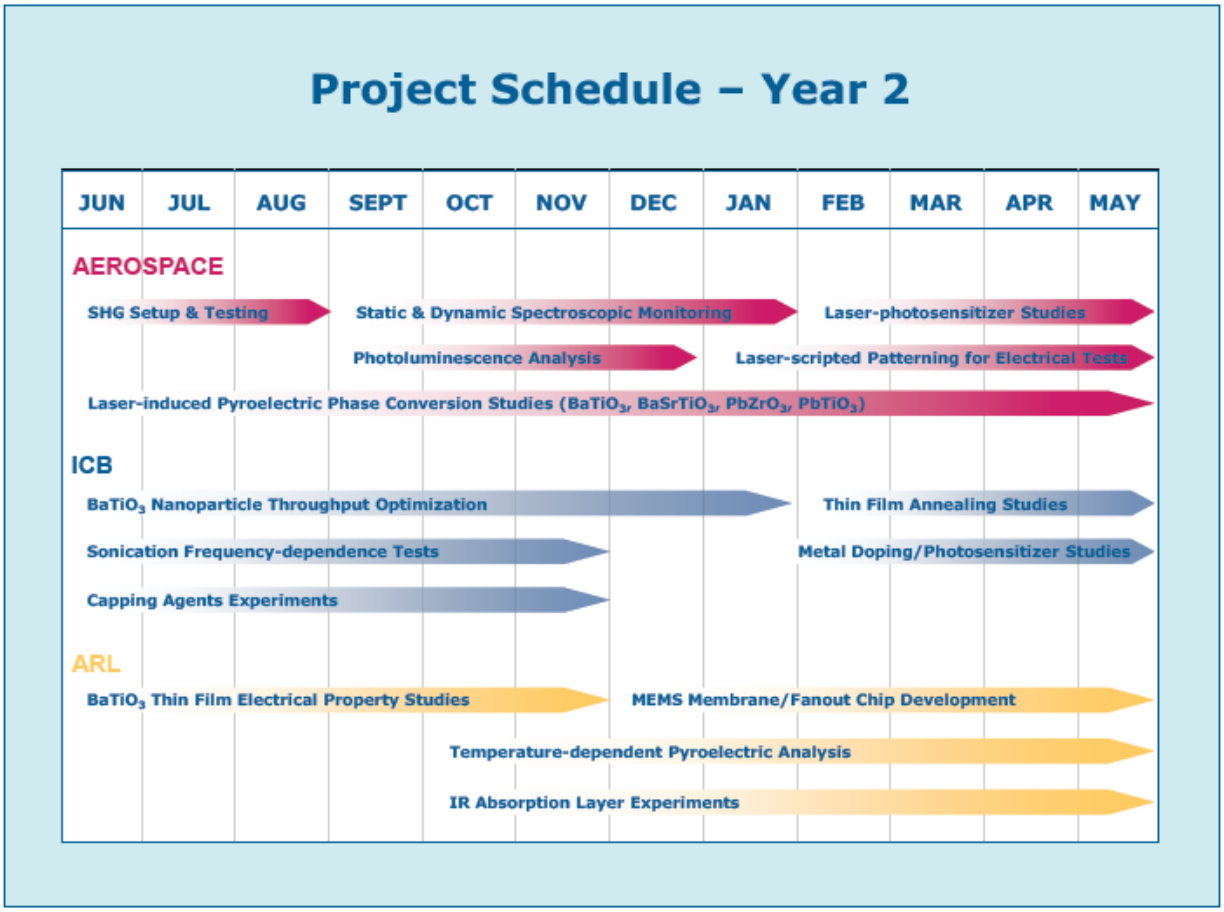

Figure 1. Project schedule.

Respective team highlights are listed in table 1.

Table 1. Highlights of Y2Q1 progress.

Aerospace	Continued investigations into the laser-induced pyroelectric cubic-tetragonal phase conversion of functionalized $BaTiO_3$ nanoparticle thin films at multiple UV wavelengths, including *laser-scripted* modulation at λ=355 nm and *intensity* modulation λ=266 nm. Efforts also focused on the development and implementation of a new dual-beam second harmonic generation (SHG) setup that permits phase conversion analysis during both static laser exposures and laser raster patterning. We expanded the capabilities of the spectroscopic detection scheme to include the ability to measure time-resolved photoluminescence during laser patterning—a distinct emission peak was observed for native $BaTiO_3$ thin films, which may prove to be a valuable direct marker for phase conversion.
ICB	Designed and built a continuous flow reactor to increase the throughput of $BaTiO_3$ synthesis. The experimental setup uses MHz frequency sonication to induce evaporation of precursor molecules in the solution, forming micro-droplets in a state of a fine mist. We are aiming to use the increased reactivity of small droplets for improved film quality and increased particle production. Experiments have been carried out to deposit films, with different thicknesses, consisting of organic acid functionalized $BaTiO_3$ nanoparticles on PtTi/Si substrates using spin coating and drop casting.
ARL	Achieved integration of electrical contacts into $BaTiO_3$ thin film structures that are a requisite for measuring critical electrical properties of the perovskite thin films, including infrared (IR) responsiveness, capacitance, and resistance, which involved evaporative deposition of TiPt and Au contacts, along with wire bonding on selective contact locations. Deposition of electrical contacts was accomplished without delamination or structural disruption of the underlying $BaTiO_3$ thin film. All project teams have accomplished their respective planned milestones for Y2Q1, and highlights of the major activities are provided in the following sections.

2. Progress by the Aerospace Corporation (Aerospace)

2.1 Laser-induced Photoemission Analysis of $BaTiO_3$ Thin Films

Our first quarter efforts for year 2 have focused on the continued development and implementation of a spectroscopic detection scheme for end-point analysis of the laser-induced pyroelectric activation and phase conversion process, where we have now investigated *photoluminescence* phenomena during intense laser irradiation as a potential marker for phase conversion. In year 1-quarter 3 (Y1Q3), we designed the optical configuration and initiated the development of an *in situ* pump-probe SHG spectroscopic detection scheme for dynamic, real-time monitoring of the pyroelectric phase conversion during laser patterning. The intent is to use the SHG activity associated with the non-centrosymmetric tetragonal polymorph to assess the extent of phase conversion from the SHG-inactive centrosymmetric cubic polymorph. In year 1-quarter 4 (Y1Q4), we expanded upon our prior efforts and designed a dual-beam experimental setup that permits the simultaneous delivery of the ultraviolet (UV) laser processing beam and IR SHG pump-beam to a substrate under dynamic patterning conditions and static exposure

conditions; these modifications will help facilitate laser pulse script optimization and refinement, along with improving process and quality control.

For the preliminary photoemission studies, we qualitatively examined the direct luminescence behavior of barium titanate thin films that were laser-irradiated at λ=266 nm under ambient temperature and pressure conditions. Figure 2 presents several photographic images that were acquired during the static laser irradiation experiments. Figure 2(a) shows the as-received cubic $BaTiO_3$/quartz sample (sample #3, 3 × 20 μl spin coat, substrate lot # Apr. 2009) prior to laser exposure. The $BaTiO_3$/quartz sample was approximately 10 mm × 10 mm and was mounted on a manual micro-XY stage assembly for sample translation and alignment. The photograph shown in figure 2(b) was captured while irradiating the $BaTiO_3$ thin film at λ=266 nm, where the laser repetition rate was 5.0 kHz, the pulse duration was τ=520 fs, and the incident per-pulse fluence was ca. 7.6 $mJ \cdot cm^{-2}$. To our surprise, the cubic phase $BaTiO_3$ thin film exhibited an intense red emission that was clearly visible to the naked eye and did not qualitatively appear to diminish with laser exposures extending to several minutes and exceeding 10^6 pulses.

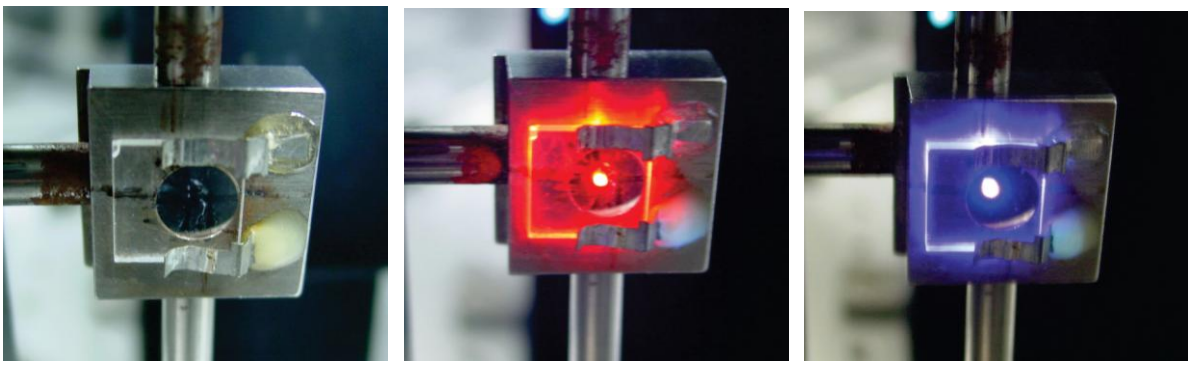

(a) (b) (c)

Figure 2. Photographs that were acquired for the static laser exposure experiments at λ=266 nm and correspond to a $BaTiO_3$/quartz sample (a) prior to laser irradiation and (b) during laser irradiation, and a quartz sample (c) during laser irradiation.

To examine whether the laser-induced photoluminescence was influenced by the underlying substrate, we also conducted laser irradiation experiments on blank quartz coupons. Figure 2(c) displays the photographic image that was acquired during laser irradiation of a quartz substrate under the same exposure conditions that were used in figure 2(b). In the absence of a $BaTiO_3$ thin film overlayer, the intense red emission was not observed, instead replaced by a strong blue emission. Clearly, the origin and behavior of the laser-induced photoluminescence phenomenon are quite different for the $BaTiO_3$/quartz sample and the quartz reference sample.

Quantitative photoemission analyses were performed by monitoring the laser-induced photoluminescence signal using an ultra-fast gated charge-coupled device (CCD) detector coupled to an Acton 300i high resolution spectrometer. Figure 3 shows the laser-induced photoluminescence results for a quartz reference sample under the same experimental conditions that were employed for the static exposure results shown in figure 2. Two discrete, intense

spectral features appear during laser irradiation at λ=266 nm, with their peaks centered at 408 nm and 532 nm, respectively. A broad, weak, and essentially featureless band also appears and is centered at approximately 650 nm. The narrow intense peak at 532 nm (bandwidth at FWHM Δλ=6 nm) does not correspond to direct photoemission, but rather relates to a first-order (2λ= 532 nm) reflection of the incident laser light from the diffraction grating inside the spectrometer. The prominent photoluminescence feature at 408 nm (bandwidth at FWHM Δλ=48 nm) corresponds to the blue light emission that was observed in figure 2, and is generally attributed to the existence of intrinsic oxygen-deficient centers (ODCs) in fused silica, which emit blue light under intense UV laser irradiation. The broad photoluminescence feature centered at ~650 nm is related to nonbridging oxygen hole centers (NBOHCs), which have been linked to plastic deformation and cracking of the glass network (*1*).

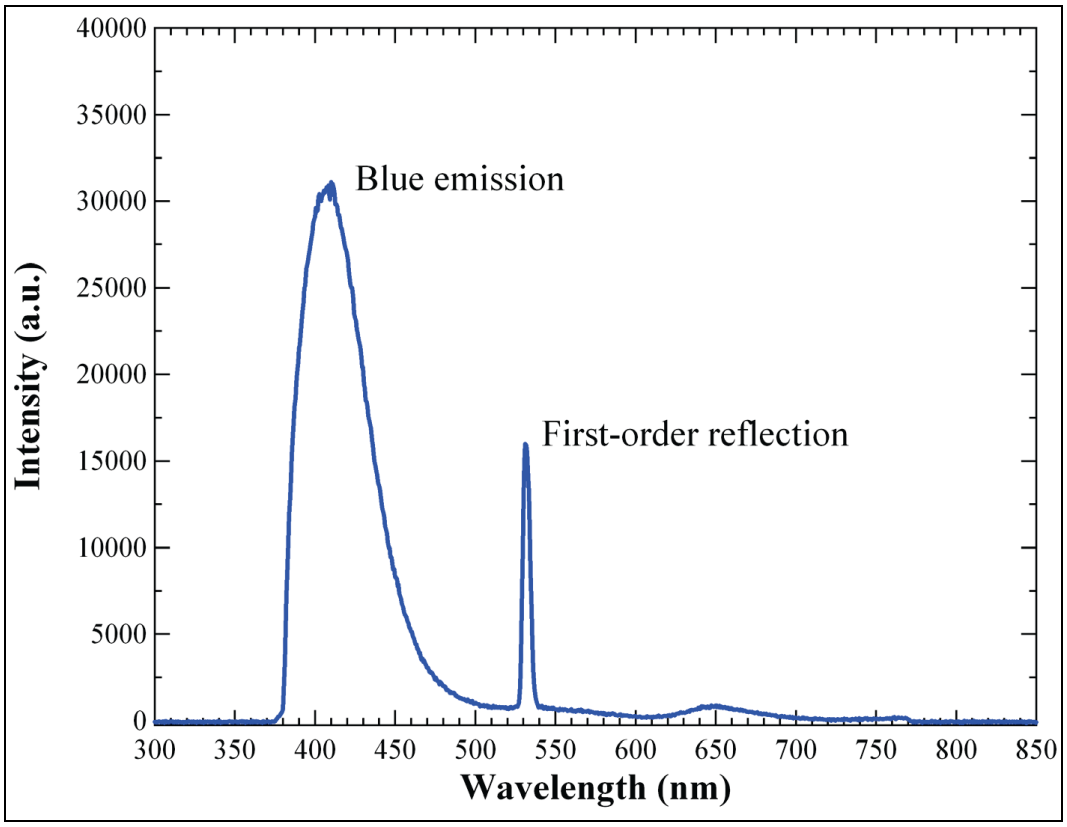

Figure 3. Photoluminescence spectrum acquired during laser irradiation (λ=266 nm) of a quartz reference sample.

Figure 4 displays the photoluminescence spectrum that was measured for the $BaTiO_3$/quartz sample (see figure 2) at λ=266 nm, where the per-pulse laser fluence was 8.0 $mJ \cdot cm^{-2}$. The laser-induced photoluminescence results reveal several important characteristics. First, the intense blue emission observed at 408 nm for the quartz substrate has been completely suppressed and is no longer detectable. Second, the first-order reflection of the incident laser light is again observed at λ=532 nm. Most important, however, is the appearance of a new distinct, intense

photoluminescence peak at 650 nm with a relatively narrow bandwidth of $\Delta\lambda$=44 nm at FWHM. This prominent photoluminescence peak is responsible for the intense red light that was detected visually (figure 2(b)), and may prove to be a valuable *direct in situ* marker for the structural phase of $BaTiO_3$. Previous photoemission studies on bulk perovskites have suggested that the origin of the photoluminescence may be related to perturbations to the fundamental octahedron unit cell, which are caused by charge transfer processes via intrinsic defects, such as oxygen vacancies, surface states, OH-defects, and non-centrosymmetric Ti^{3+} ions (*2*).

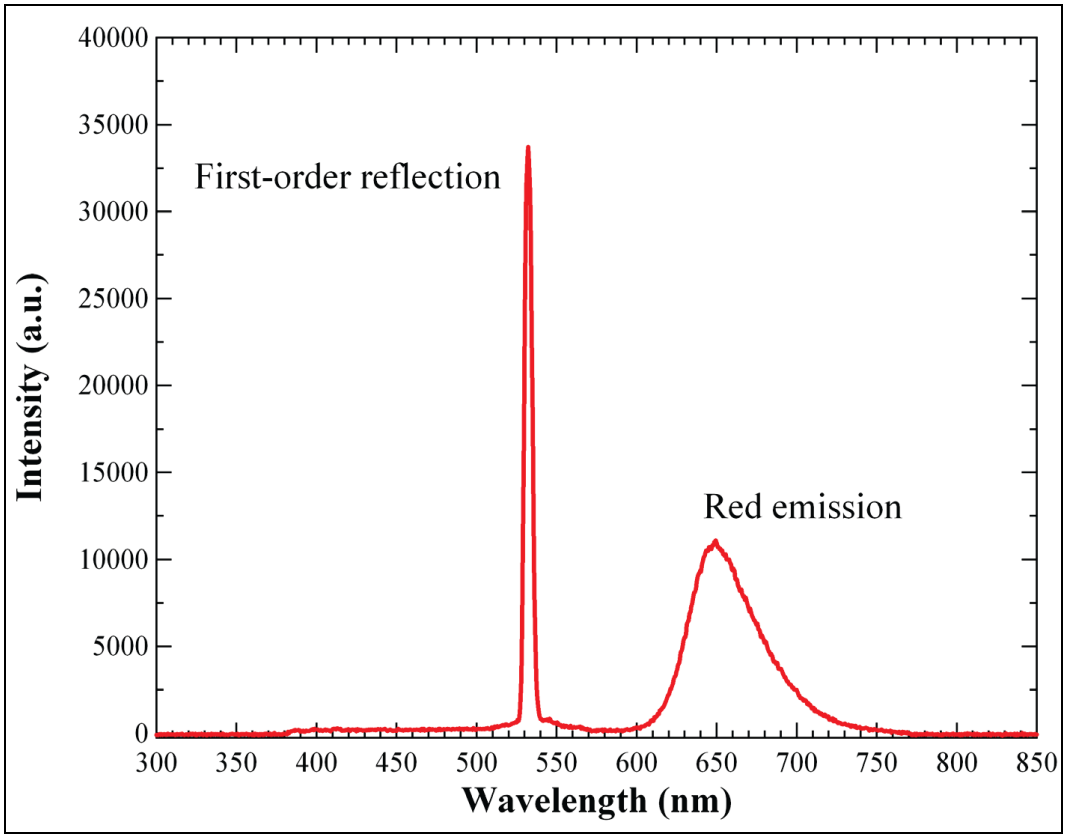

Figure 4. Photoluminescence spectrum acquired during laser irradiation (λ=266 nm) of a $BaTiO_3$ thin film deposited on a quartz substrate.

We have also investigated the fluence dependence of the 650 nm photoemission feature to assess whether the laser-induced photoluminescence is a single photon or multiple photon process. Figure 5 shows the measured photoluminescence intensity versus wavelength at incident laser fluences that ranged from $F=1.5x10^{-2}$ mJ·cm^{-2} to F=5.2 mJ·cm^{-2}. The emission results indicate that the 650 nm photoluminescence intensity increases with incident laser fluence, while the peak maximum location remains unchanged over the range of fluencies studied. The inset in figure 5 displays the integrated peak areas for the 650 nm feature versus incident laser fluence. A third-order polynomial fit is provided as a visual guide, and the multiple photon dependence is consistent with a non-linear excitation process via intense ultra-fast pulse laser irradiation of the $BaTiO_3$ thin film.

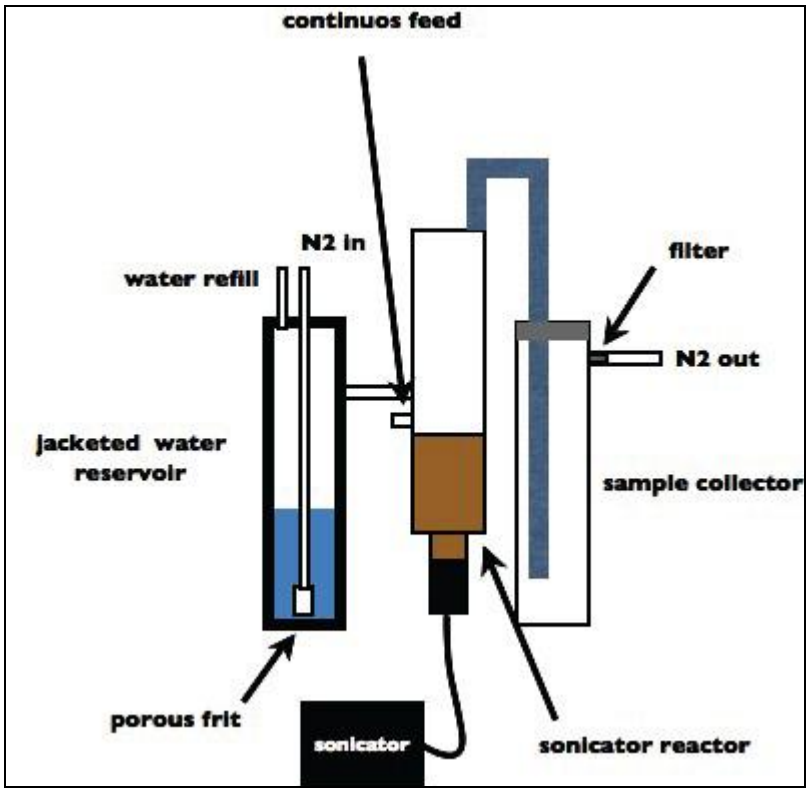

Figure 5. Schematic of the reactor setup for continuous production of $BaTiO_3$ nanoparticles by sonication-induced evaporation.

In the next quarter, we will investigate the photoluminescent properties of $BaTiO_3$ thin film samples that have undergone controlled thermal treatment via conventional furnace heating and laser-scripted processing at multiple UV wavelengths. Our aim is to determine if thermal processing and cubic-tetragonal phase conversion produce photoemission features that are in marked contrast to the as-received native $BaTiO_3$ samples. If successful, this photoluminescence approach will simplify the *in situ* detection of the pyroelectric phase transformation since an additional pump-beam (IR SHG) is not required for second harmonic generation; in this new scenario, the UV laser processing beam would be responsible for inducing the structural phase change, as well as promoting photoluminescence.

3. Institute for Collaborative Biotechnologies (ICB)

3.1 Continuous Flow Reactor by Sonication Induced Vaporization

The experimental setup (figure 6) consists of three individual and well-separated glass parts. The first part is a dual-jacketed reactor filled with diluted hydrochloric acid (0.75 M), which will provide the reaction with the catalyst vapor by bubbling inert gas through it. The catalyst vapor meets with the alkoxide precursor in the 2nd chamber, where the single source BaTi double

metal alkoxide is vaporized by a sonicator operated at 1.6 MHz frequency to form a fine mist containing micron-sized droplets. From this point, the mixed vapor (catalyst/alkoxide) is driven into the third vessel, which is the sample collector, by the inert gas flow. The system is currently under testing.

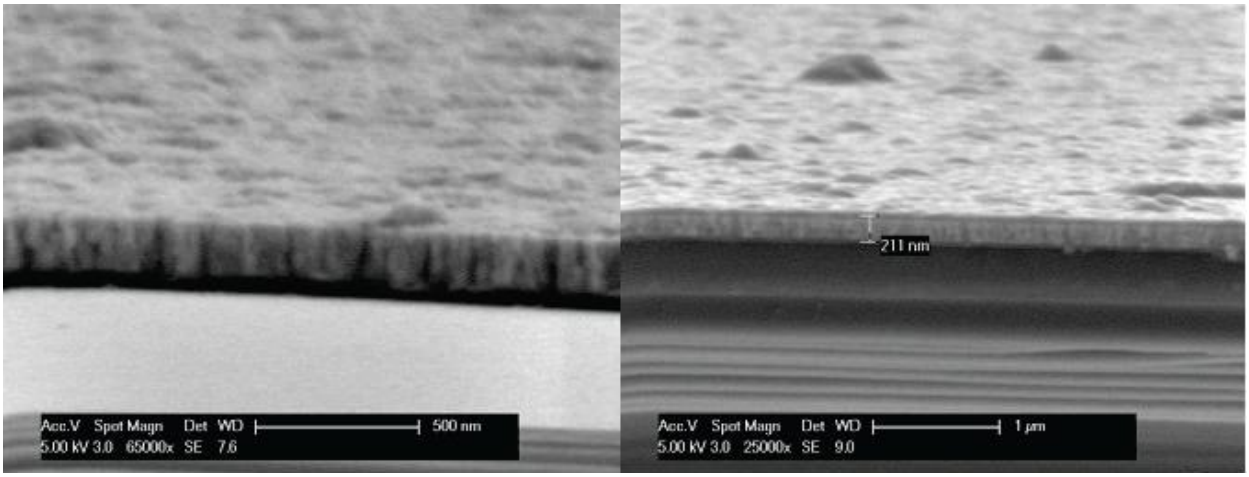

Figure 6. SEM images of $BaTiO_3$ films featuring 210 nm thickness prepared by spin coating.

We believe that this combination of sonication induced vaporization and the original idea of low-temperature vapor diffusion catalysis offers several advantages, which will help us to move towards continuous production of valuable materials, such as the $BaTiO_3$ nanoparticles. These advantages include the following:

1. MHz frequency sonication produces small droplets, including the alkoxide pool, with high specific surface area.

2. The flow rate of the carrier inert gas is tunable, and if chosen appropriately, it could provide enough time to facilitate the mixing and the reaction of the basic ingredients before reaching the collector vial and the gas outlet.

3. The throughput of the synthesis method highly depends on, among other factors, the maximum of the vaporization rate of the transducer, which is given as 10 mL/min with water.

3.2 Preparation of $BaTiO_3$ Films for Studying Laser-induced Site-selective Transformation

$BaTiO_3$ thin films featuring different thicknesses were deposited on platinum titanium (PtTi)/ silicon (Si) substrates and sent to Aerospace for laser-induced site-selective transformation experiments. Our aim was to produce a series of samples featuring thickness in the range of a few hundred nanomicrons up to few microns. The samples were prepared by spin coating and drop casting the surface functionalized $BaTiO_3$ particles from hexane solution. During the spin coating experiments, the spinning speed and the ramp rate were varied between 1,500–6,000 RPM and 200–1000 RPM/s, respectively. Spin coating using 6,000 RPM for 30 s and

1,000 RPM/s ramp rate, resulting in a uniform film with around 210 nm thickness (figure 7); this thickness was identified as best to form good quality films reproducibly and consistently.

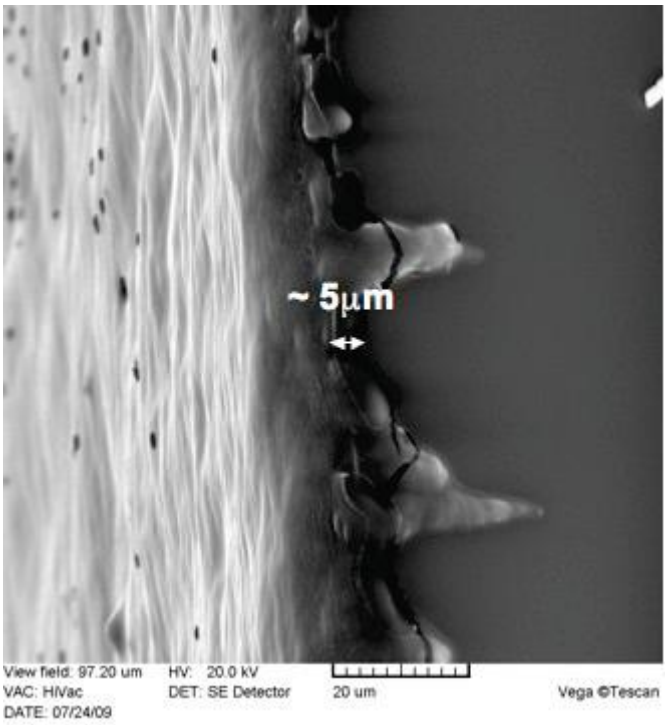

Figure 7. SEM image of $BaTiO_3$ films featuring 5 μm thickness prepared by drop casting.

We observed a more than 50% increment in thickness from around 210 nm to 350 nm when the spinning speed was decreased from 6,000 RPM to 1,500 RPM. However, the film prepared at lower spinning speed was also characterized with larger surface roughness and, therefore, undesired film morphology.

Subsequent deposition of $BaTiO_3$ nanoparticles by spin coating at 6,000 RPM resulted in only doubling the film thickness (210 nm–450 nm) after 10 cycles, but the surface morphology did not changed significantly this time.

The most reliable way to produce relatively smooth films with thickness in the micrometer range was through drop casting 20 μL of the mother $BaTiO_3$/hexane suspension, followed by drying carried out at 50 ^oC (figure 8).

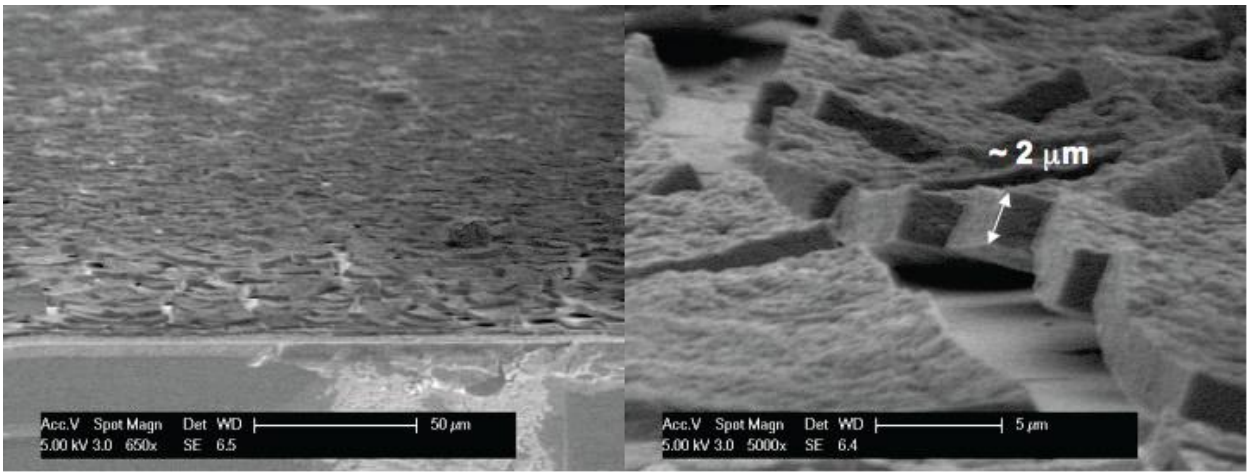

Figure 8. SEM images of $BaTiO_3$ films featuring 2 μm thickness prepared by drop casting and subsequent annealing at 300 °C.

In order to make the films more compact, and to remove the embedded hexane and—at least partially—the hydrocarbon residue from the organic capping, an annealing process at 300 ^oC was carried out. Although the annealing attempts resulted in significant compression of the film (figure 9) from 5 μm to around 2 μm in thickness, an intensive cracking through the film was also observed.

Figure 9. $BaTiO_3$/TiPt/Si multilayer structure.

From our results based on the experiments with different depositions techniques, we can conclude that spin coating at high spinning speed and using high ramp rate is necessary to produce good quality thin films. However the fabrication of robust, thicker films with satisfying surface roughness and morphology still remains a challenging task for the future.

3.3 Future Tasks

Continuous synthesis process:

1. Carry out experiments to test the capability of the system to produce well-defined $BaTiO_3$ nanoparticles.
2. Determine the maximum throughput of the system.
3. Investigate the sonication frequency dependency of the final product morphology by other tunable transducers in the 550 kHz–1.6 MHz frequency range.

4. Explore the effects of including capping agents during $BaTiO_3$ nanoparticle synthesis to achieve even better dispersion of the particles in films, more uniform packing, and stronger adhesion.

Film deposition:

5. Investigate the annealing process to produce thick and dense $BaTiO_3$ films, while preserving process continuity.
6. Study the possibility of using larger wafers for depositions.
7. Carry out fundamental investigations of fabricating lead zirconate ($PbZrO_3$) (PZ)-, lead titanate ($PbTiO_3$) (PT)-, and $Pb(Ti,Zr)O_3$ (PZT)-contained thin films for optimizing the pyroelectric perovskite layer in the IR detector.

4. Progress by the Army Research Laboratory (ARL)

4.1 Preparation for Electrical Characterization Measurements

The quality of the $BaTiO_3$ films provided by the ICB has improved to the point that we could begin electrical characterization. We supplied the ICB with Si wafers with an evaporated layer of TiPt on the surface. The TiPt serves as the bottom electrical contact and also improves the cohesion of the $BaTiO_3$ to the substrate. ICB deposited $BaTiO_3$ layers of varying thicknesses onto several substrates (figure 10) and sent the samples back to ARL.

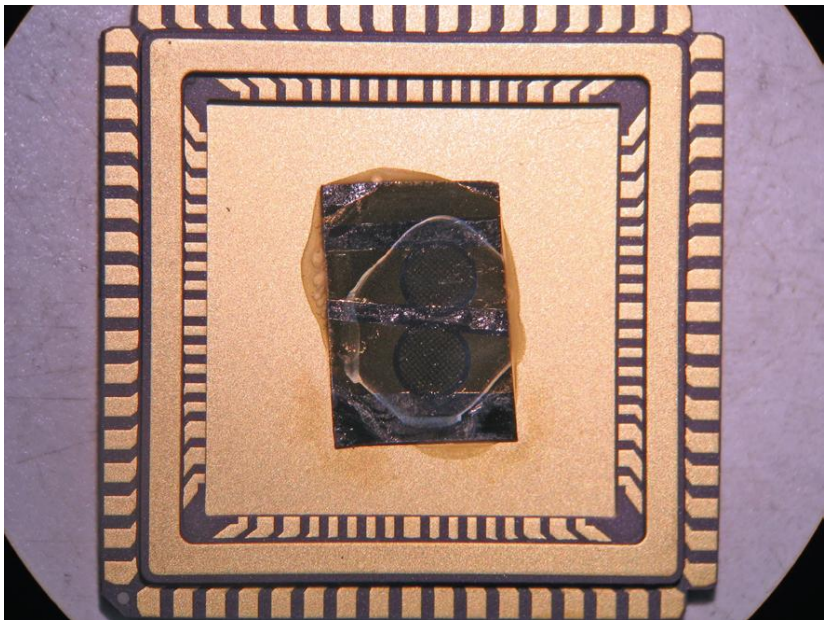

Figure 10. $BaTiO_3$ thin film following the application of a top electrical contact.

We then applied a top electrical contact to the $BaTiO_3$ film, as shown in figure 11. The top contact had to be patterned (there should be small areas of material with a deposited metallic layer surrounded by material with a "bare" surface). We used a 3 mm transmission electron microscope (TEM) copper grid with 100-micron holes as a mask. Two grids were taped onto the film with Kapton tape. Tape was also placed at the ends of the sample. The sample was then placed into the evaporator and a 250 Å chromium (Cr) adhesion layer was deposited, followed by a 2500 Å gold (Au) contact layer. The Kapton tape and the grids were removed, thus exposing the film and leaving behind a pattern of top contacts (figure 11). In the four corners of the sample, the film was removed to expose the bottom TiPt contact. The images show that the sample is mounted onto a 68-pin leadless chip carrier (LCC). This is a type of packaging for integrated circuits, and is standard for packaging focal plane arrays (FPAs).

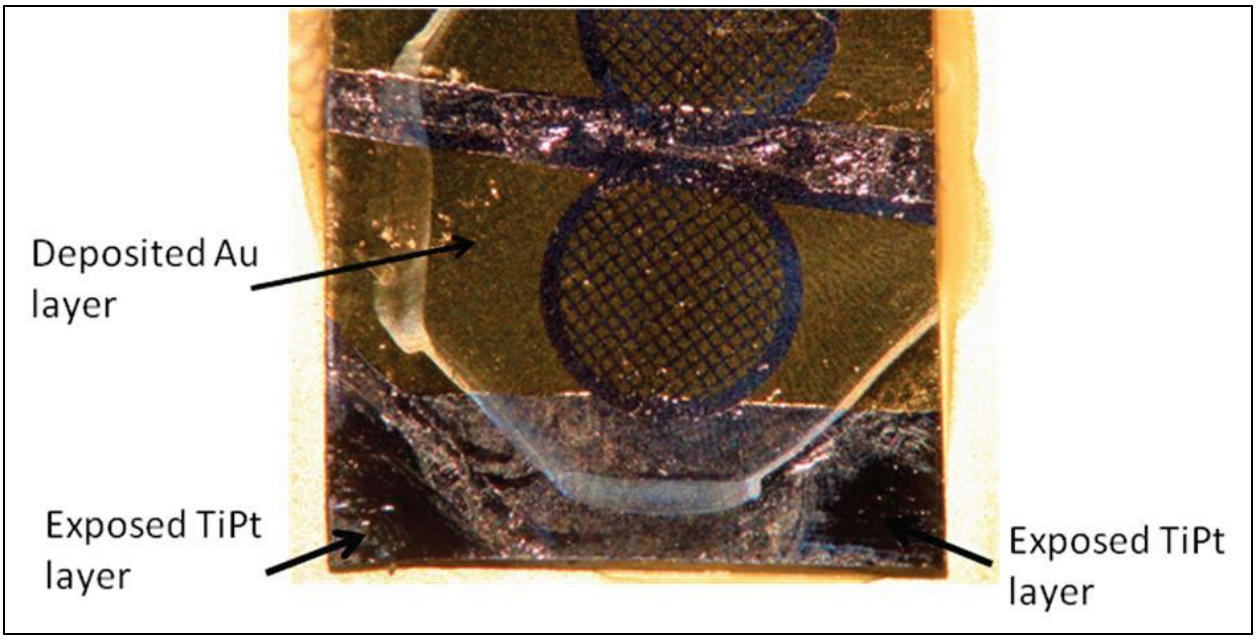

Figure 11. Close-up view of the $BaTiO_3$ thin film showing the top electrical contact grid pattern.

The next step was to wire bond some of the square Au regions and the four exposed TiPt regions, so that we could measure properties such as capacitance and resistance. A wire-bonded $BaTiO_3$ film is shown in figure 12. The film stood up to the process. A common failure mode would be for the film to lift off during the bonding process, or for the bond to not "stick." The $BaTiO_3$ film is in its as-grown cubic polycrystalline phase. After making baseline measurements with this film, we will induce the phase transformation to the pyroelectrically active tetragonal phase. If the film is pyroelectrically active, it will have a temperature-dependent capacitance. We will test $BaTiO_3$ that has undergone phase transformation via the laser processing method in the same manner.

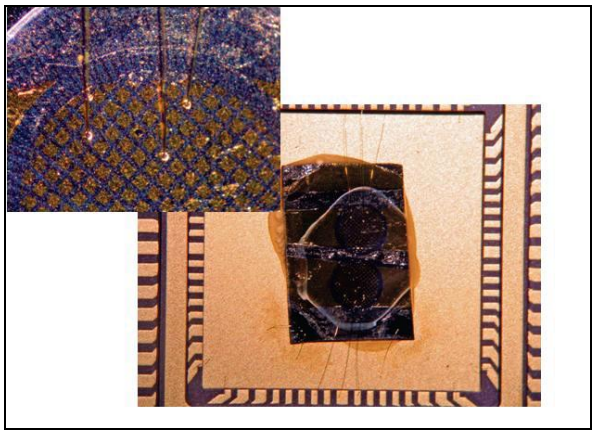

Figure 12. $BaTiO_3$ thin film following the application of wire bonds.

4.2 IR Absorption Layer Research

In this quarter, we also began planning for the IR absorption layer that will need to go on top of the structure. For our thermal detector project, we need a layer similar to a thin coating of black paint that absorbs a wide range of wavelengths and heats up. The heat is transferred to the $BaTiO_3$ layer, and a pyroelectric voltage is generated. A candidate that is compatible with some of the MEMS processing, and will be required for the actual detectors, is a thin layer of black Si. We have developed a technique (figure 13) that uses metal nanoparticles and dry etching to generate the nanopillars in the Si surface that traps light of a wide range of wavelengths (independent of the bandgap of the Si), most of which will be absorbed by free electrons and turned into heat.

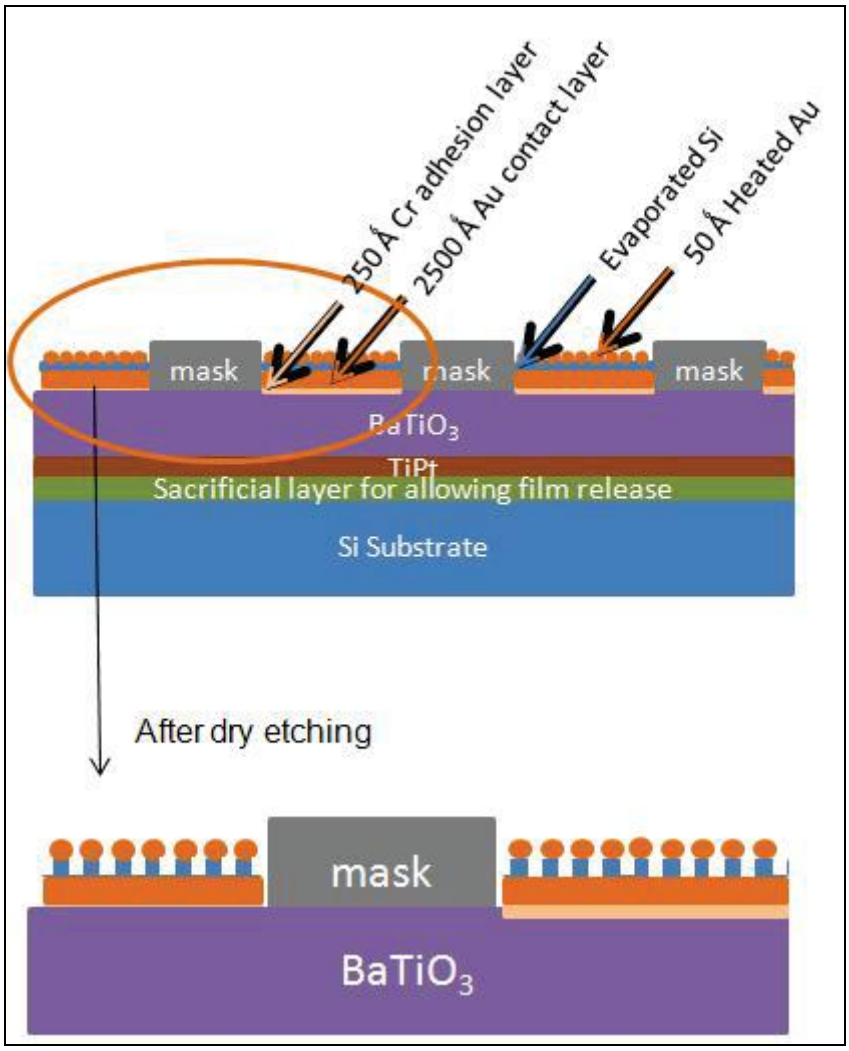

Figure 13. Dry etch approach to the fabrication of black silicon nanopillars for enhanced IR absorption.

5. Plans and Goals for Year 2 Quarter 2

In the coming quarter, we will continue to expand our nanomaterial synthesis capabilities, laser processing techniques and spectroscopic phase conversion studies, and perovskite thin film electrical characterization efforts. We also intend to initiate and pursue several new areas of focus. ICB will explore the effects of including capping agents during $BaTiO_3$ synthesis to further enhance particle dispersion, and perform fundamental investigations of fabricating lead oxide thins films (e.g., $PbZrO_3$ and $PbTiO_3$) for optimizing the pyroelectric perovskite layer in the IR detector. Aerospace will conduct photoluminescence studies on UV laser-processed and furnace-treated $BaTiO_3$ thin films to explore the possible existence of a direct optical marker for pyroelectric phase transformation control; it will also expand our laser scripted processing

studies to include other nanostructured thin films that are important for uncooled IR detector technologies, such as $Ba_xSr_{1-x}TiO_3$ and Sr_xBa_{1-x} Nb_2O_6. ARL will perform electrical characterization and temperature-dependent pyroelectric measurements on ICB-provided functionalized BaTiO3 thin films, and investigate the use of black Si nanopillar structural layers for enhanced IR absorption.

6. Metrics for Year 2 Quarter 1

1. W. L. Sarney, J. W. Little, F. E. Livingston, K. Niesz, D. E. Morse, and M. W. Cole, Low temperature growth and laser-induced phase transformation of BaTiO3 films for uncooled IR detector applications, poster accepted for presentation at the 2009 Materials Research Society (MRS) Meeting, Boston, MA, Nov. 30–Dec. 4.

2. F. E. Livingston, W. L. Sarney, K. Niesz, and D. E. Morse, "Laser-induced structuring of bio-inspired nanomaterials for sensor technology applications," accepted for presentation as an invited talk at the 2010 Military Sensing Symposia (MSS), Materials/Detectors Joint Session: Uncooled IR Detector and FPA Technology, Orlando, FL, Feb. 22–26.

7. References

1. Zoubir, A.; Rivero, C.; Grodsky, R.; Richardson, K.; Richardson, M.; Cardinal, T.; Couzi, M. *Phys. Rev. B* **2006**, *73*, 224117.
2. Zhang, M.-S.; Yin, Z.; Chen, Q.; Zhang,W.; Chen, W. *Solid St. Commun.* **2001**, *119*, 659.

List of Symbols, Abbreviations, and Acronyms

ARL	U.S. Army Research Laboratory
BaTiO3	barium titanium oxide
BST	barium strontium titanate
CCD	charge-coupled device
Cr	chromium
fs	femtosecond
FPA	focal plane array
ICB	Institute for Collaborative Biotechnologies
IR	infrared
nm	nanometer
$PbZrO_3$	lead zirconate
$PbTiO_3$	lead titanate
SHG	second harmonic generation
Si	silicon
TiPt	titanium platinum
UV	ultraviolet
Y1Q4	year one, quarter four
Y2Q1	year two, quarter one
Y2Q2	year two, quarter two
Y1Q3	year one, quarter three

NO. OF COPIES	ORGANIZATION
1 ELEC	ADMNSTR DEFNS TECHL INFO CTR ATTN DTIC OCP 8725 JOHN J KINGMAN RD STE 0944 FT BELVOIR VA 22060-6218
1 CD	OFC OF THE SECY OF DEFNS ATTN ODDRE (R&AT) THE PENTAGON WASHINGTON DC 20301-3080
1	US ARMY RSRCH DEV AND ENGRG CMND ARMAMENT RSRCH DEV & ENGRG CTR ARMAMENT ENGRG & TECHNLGY CTR ATTN AMSRD AAR AEF T J MATTS BLDG 305 ABERDEEN PROVING GROUND MD 21005-5001
1	PM TIMS, PROFILER (MMS-P) AN/TMQ-52 ATTN B GRIFFIES BUILDING 563 FT MONMOUTH NJ 07703
1	US ARMY INFO SYS ENGRG CMND ATTN AMSEL IE TD A RIVERA FT HUACHUCA AZ 85613-5300
1	COMMANDER US ARMY RDECOM ATTN AMSRD AMR W C MCCORKLE 5400 FOWLER RD REDSTONE ARSENAL AL 35898-5000
1	US GOVERNMENT PRINT OFF DEPOSITORY RECEIVING SECTION ATTN MAIL STOP IDAD J TATE 732 NORTH CAPITOL ST NW WASHINGTON DC 20402
2	INSTITUTE FOR COLLABORATIVE BIOTECHNOLOGIES UNIVERSITY OF CALIFORNIA, SANTA BARBARA ATTN D MORSE ATTN K NIESZ SANTA BARBARA CA 93106-5100

NO. OF COPIES	ORGANIZATION
1	THE AEROSPACE CORPORATION MICRO/NANOTECHNOLOGY DEPARTMENT SPACE MATERIALS LABORATORY ATTN F LIVINGSTON 2350 E EL SEGUNDO BLVD EL SEGUNDO CA 90245
1	US ARMY RSRCH LAB ATTN RDRL CIM G T LANDFRIED BLDG 4600 ABERDEEN PROVING GROUND MD 21005-5066
6	US ARMY RSRCH LAB ATTN IMNE ALC HRR MAIL & RECORDS MGMT ATTN RDRL CIM L TECHL LIB ATTN RDRL CIM P TECHL PUB ATTN RDRL SEE I J LITTLE ATTN RDRL SEE I K OLVER ATTN RDRL SEE I W SARNEY ADELPHI MD 20783-1197

TOTAL: 17 (1 ELEC, 1 CD, 15 HCS)

INTENTIONALLY LEFT BLANK.